JOURNAL OF GEOPHYSICAL RESEARCH, VOL. 98, NO. B10, PAGES 17,667–17,682, OCTOBER 10, 1993

Flow of Ices in the Ammonia-Water System

W. B. DURHAM

Lawrence Livermore National Laboratory, University of California, Livermore

S. H. KIRBY AND L. A. STERN

U.S. Geological Survey, Menlo Park, California

We have fabricated in the laboratory and subsequently deformed crystalline hydrates and partial melts of the water-rich end of the NH_3-H_2O system, with the aim of improving our understanding of physical processes occurring in icy moons of the outer solar system. Deformation experiments were carried out at constant strain rate. The range of experimental variables was strain rate $3.5 \times 10^{-7} < \dot{\varepsilon} < 3.5 \times 10^{-4}$ s^{-1}, temperature $132 < T < 220$ K, pressure $50 \leq P \leq 100$ MPa, and mole fraction NH_3 $0 \leq x_{NH_3} \leq 0.295$. Phase relationships in the NH_3-H_2O system indicate that water ice and ammonia dihydrate, $NH_3 \cdot 2H_2O$, are the stable phases under our experimental conditions. X ray diffraction of our samples usually revealed these as the dominant phases, but we have also observed an amorphous phase (in unpressurized samples only) and occasionally significant ammonia monohydrate, $NH_3 \cdot H_2O$. The onset of partial melting at the peritectic temperature at about 176 K appeared as a sharp transition in strength observed in samples of $x_{NH_3} = 0.15$ and 0.295. In samples of $x_{NH_3} = 0.05$ and 0.01, the effect of melt was less pronounced. For any given water ice + dihydrate alloy in the subsolidus region, we observed one rheological law over the entire temperature range from 176 K to about 140 K. Below 140 K, a shear instability similar to that occurring in pure water ice under the same conditions limited our ability to measure ductile flow. The rheological laws for the several alloys vary systematically from that of pure ice to that of dihydrate. Pure dihydrate is about 4 orders of magnitude less viscous than water ice just below the peritectic temperature, but because of a very pronounced temperature dependence in dihydrate (100 kJ/mol versus 43 kJ/mol for water ice) the viscosity of dihydrate equals or exceeds that of water ice at $T < 140$ K. The large variation in viscosity of dihydrate with relatively small changes in temperature may be helpful in explaining the rich variety of tectonic and volcanic features seen on the surfaces of icy moons in the outer solar system.

INTRODUCTION

Among the volatiles condensing from the solar nebula, ammonia must be considered as one of the important constituents of satellites of the outer solar system. Given reasonable assumptions about the composition of the solar nebula and the distillating effects of condensation in a temperature gradient and the kinetics of chemical reactions in protoplanetary nebulae, it is reasonable to expect bulk ammonia-to-water ratios in the moons of Saturn and beyond to be of the order of 0.15 [*Lewis*, 1972; *Prinn and Fegley*, 1981]. The icy moons have not always been quiescent, based on images from the Voyager missions. Signs of volcanism and a variety of tectonic activity, some with terrestrial analogs and some quite extraordinary, are abundant on both large and small moons (see *Smith et al.* [1989] and references therein to earlier reports by the Voyager imaging team). The Voyager images show no gradient in tectonic activity on icy satellites with distance from the Sun, implying either that the satellites were at about the same temperature when the tectonic activity occurred, which seems unlikely, or that there is a compositional gradient towards lower-melting-temperature solids with increasing solar radius.

In order to constrain several of the parameters used for modeling planetary evolution and ongoing tectonic activity and surface relaxation, we have performed mechanical tests on likely planetary materials under environmental conditions of pressure, temperature, and strain rate that are relevant to satellite conditions. This paper reports our measurements for solids and partial melts in the system NH_3-H_2O. Ammonia dihydrate, $NH_3 \cdot 2H_2O$, is the stable NH_3-bearing phase of the water-rich portion of the NH_3-H_2O system below 1 GPa pressure [*Boone and Nicol*, 1991], and is of particular planetological interest because it melts at approximately 176 K, even when alloyed with water ice. Furthermore, the first melt to form in the water ice + dihydrate system has approximately the dihydrate composition, leading to the possibility of fractionation and concentration of low-melting-temperature materials on icy moons where ammonia is present. Among the satellites where NH_3-H_2O ices may be of particular importance are those with a radius of a few hundred kilometers or less, which are therefore less capable of generating high internal temperatures than the icy giants. It is suspected that some of the activity that occurred on these smaller and colder moons is due to the presence of solids, such as the hydrates of ammonia, with melting temperatures far below that of water ice [e.g., *Consolmagno*, 1983].

In retrospect the experiments also have an important terrestrial application in that they explore the deformation of two-phase systems over a spectrum of compositions and contrasting rheologies. A few specific terrestrial assemblages have been investigated in the past, but general treatments are still mainly theoretical [see *Tullis et al.*, 1991, and references therein]. Because the flow of water ice and dihydrate turn out to have sharply different temperature sensitivities, viscosity contrasts of zero to 4 orders of magnitude can be prescribed by the appropriate selection of temperature, and since the full spectrum of sample compo-

Paper number 93JB01564.
0148-0227/93/93JB-01564$05.00

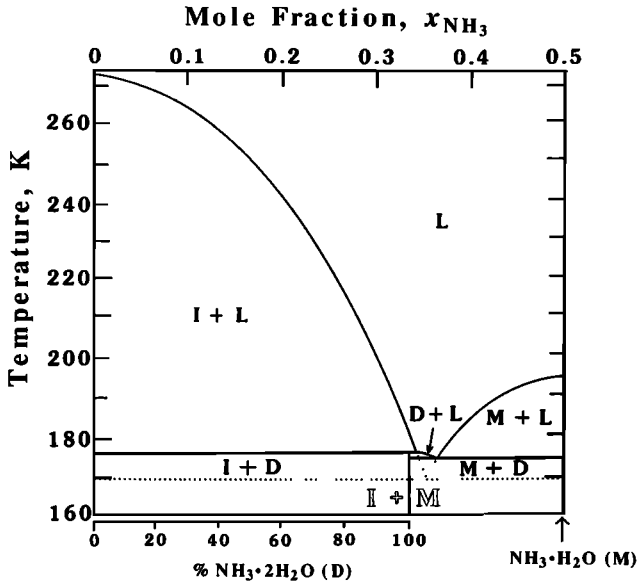

Fig. 1. Phase diagram for the system NH_3-H_2O at one atmosphere pressure for ammonia mole fraction $x_{NH_3} \leq 0.5$. The overall phase relations are taken from *Rollet and Vuillard* [1956], but the invariant points of the ammonia hydrates are from *Hildenbrand and Giauque* [1953] and *Chan and Giauque* [1964]. The metastable ice-monohydrate eutectic is shown by the dotted lines.

sitions from pure water ice to pure dihydrate can be fabricated, the opportunity exists to test the theories much more generally than has been possible with earth materials.

Phase Relations in the System NH_3-H_2O and Sample Preparation

Figure 1 is the phase diagram for the water-rich half of the NH_3-H_2O system at 0.1 MPa, plotted as mole fraction ammonia x_{NH_3} versus temperature. Prominent is the very steep depression of the liquidus from 273.15 K at $x_{NH_3} = 0$ to 175.4 K at $x_{NH_3} = 0.365$, a nearly 100-K drop in the melting point. No appreciable solid solution of ammonia in ice or between the hydrates has been detected (see the short review by *Cynn et al.* [1989]). Ice I progressively crystallizes with cooling from melts of composition $x_{NH_3} < 0.340$ over a broad temperature interval until the peritectic temperature, $T_p = 176.1$ K, is reached. At this point the remaining liquid of composition $x_{NH_3} = 0.340$ reacts with some of the ice to form ammonia dihydrate ($x_{NH_3} = 0.333$), yielding the subsolidus phases water ice + ammonia dihydrate for bulk compositions of $x_{NH_3} < 0.333$. For melt compositions $0.500 > x_{NH_3} > 0.333$, the stable subsolidus phases are dihydrate and ammonia monohydrate, $NH_3 \cdot H_2O$, with final crystallization occurring at the eutectic temperature, 175.4 K. Our test pressures (50 to 100 MPa) are expected to change the diagram only slightly in the vicinity of the peritectic point: the (metastable) congruent melting temperature of dihydrate is about 2.6 to 5.6 K higher at 100 MPa than 0.1 MPa, and the bulk composition at the peritectic also shifts only slightly (see the summary of the high-pressure phase relations of *Cynn et al.* [1989] and thermodynamic data of *Croft et al.* [1988]). Although the thermodynamically stable crystalline phases for compositions of $x_{NH_3} < 0.333$ are ammonia dihydrate and water ice, metastable phases may occur in this compositional range at temperatures below T_p; ammonia monohydrate may be produced as a subsolidus phase from a metastable eutectic forming directly between ice and monohydrate at $x_{NH_3} = 0.35$ and $T = 169.8$ K (Figure 1, dotted line), and $NH_3 \cdot nH_2O$ glasses may form from supercooling of melts of the same composition [*Rollet and Vuillard*, 1956; *Van Kasteren*, 1973; *Bertie and Shehata*, 1984; *Kargel et al.*, 1991].

A detailed description of our sample synthesis method is presented here in order to explain how the equilibrium dihydrate phase was grown in spite of these problems of metastability. We exploited the phase relations for the ammonia-water system shown in Figure 1 in making polycrystalline water ice–ammonia hydrate alloys of composition $x_{NH_3} < 0.333$ with controlled grain size by the following procedure.

Analogous to our method for molding polycrystalline water ice samples [*Durham et al.*, 1983], we packed seed ice into cylindrical molds with the desired 25-mm inner diameter, evacuated the molds to 0.1 Pa Hg, backfilled with ammonia-water liquid to saturate the pores between the seed crystals, then slowly lowered the temperature of the assembly to below the dihydrate-monohydrate eutectic. To fabricate ammonia-water samples with compositions $x_{NH_3} = 0.01$, 0.05, and 0.15, we used crushed and sieved triply distilled water ice seed material (0.25–0.6 mm grain size) packed into a stainless steel (316) molding tube to a reproducible porosity of 0.50 ± 0.05, then admitted a liquid mixture of water plus concentrated ammonium hydroxide solution ($x_{NH_3} = 0.295 \pm 0.005$). The composition of the liquid was chosen to achieve a desired final bulk composition of the sample. The initial temperature T_i at which the liquid was introduced into the molds was the liquidus temperature for the bulk composition (based on Figure 1). For example, to make a sample of final bulk composition $x_{NH_3} = 0.05$, we used a liquid of $x_{NH_3} = 0.10$ and started at $T_i = 269$ K. Nearly pure dihydrate samples were made by freezing $x_{NH_3} = 0.295$ ammonium hydroxide solution in the molding tube with no added seed ice. Two chromel-alumel thermocouples were attached to the base and side of the molding tube to monitor temperature, and an insulating closed-foam sleeve was placed around the molding tube and the thermocouples. The assembly was then placed in a steel cannister suspended above a liquid nitrogen bath for controlled freezing.

Samples were slowly cooled from the liquidus temperature through the ice-dihydrate peritectic, then warmed and cycled through the peritectic temperature several times and finally cooled very slowly down to 77 K (approximately 6–7 hours, total) for storage. The foam sleeve insulating the sides of the sample promoted freezing from bottom to top, and the upwardly moving freezing front helped exclude trapped gas in the system. Prior to mechanical testing, samples were removed from storage, shaved flat and square at their ends, and sealed in thin-walled indium capsules.

Cooling of the seed ice + liquid mixture below the peritectic temperature T_p should, if equilibrium is obtained, result in crystallization of dihydrate. X ray patterns of the as-molded samples show that this is not the case: the water ice peaks always appear clearly, but broad scattering centered around $2\theta = 25°$ indicates that an amorphous NH_3-bearing phase, probably glass, was formed with only minor crystalline ammonia hydrates (Figure 2*b*). This is in spite of very slow cooling rates (about 3 hours to cool from T_i to below T_p) and slow cycling several times across the T_p, a

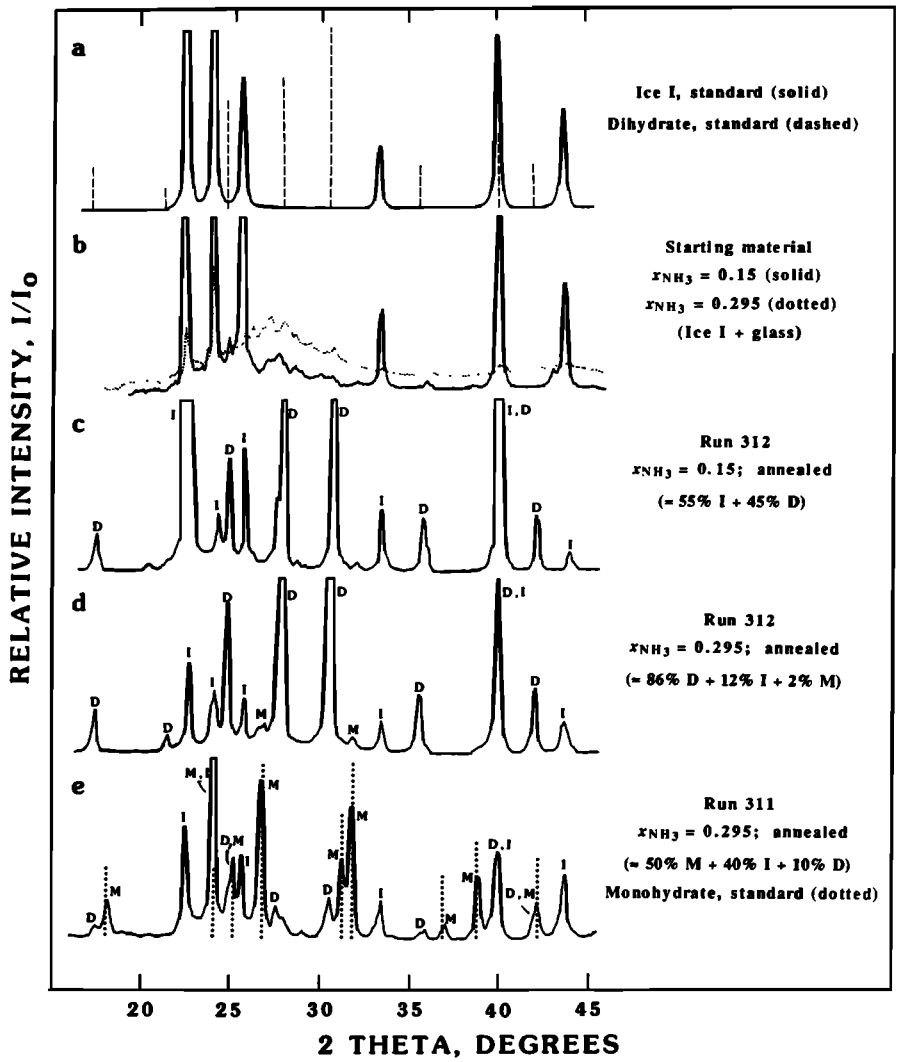

Fig. 2. X ray diffraction patterns of reference, as molded, and pressurized-only samples. Cu K_α radiation. Sample temperatures were near 77 K.

practice that can promote growth of dihydrate from glass in small-volume samples [*Bertie and Shehata*, 1984]. However, we found that pressurizing samples for a relatively (to typical run times) brief 30 min at characteristic run temperatures devitrifies the amorphous phase to fine-grained dihydrate with monohydrate minor or absent as an accessory phase (Figures 2*c* and 2*d*). This devitrification is evidently driven by the small volume reduction that accompanies the process (about −1.8% [*Croft et al.*, 1988]). X ray evidence for an amorphous phase was absent from these pressurized-only samples as well as from any deformed samples. Thus we conclude that the amorphous ammonia-water phase was reduced to below detection limits (<1%) by the hydrostatic pressurization prior to sample deformation and played no role in the deformation behavior. Ammonia dihydrate peaks were identified from X ray diffraction data given by *Bertie and Shehata* [1984], and the locations of ammonia monohydrate peaks were calculated from crystal structure data given by *Olovsson and Templeton* [1959].

Ammonia monohydrate has been produced in some of the samples. It appeared in substantial proportions (relative to total NH_3 concentration) in the X ray patterns of deformed samples with $x_{NH_3} = 0.05$ and in trace amounts in some of the samples with $x_{NH_3} = 0.15$ and 0.295 (Table 1). Samples that were warmed above T_p and then recooled (either prior to pressurization or under pressure) sometimes produced more monohydrate than dihydrate (Figure 2*e*), a phenomenon that may be associated with initial nucleation of monohydrate at the metastable eutectic. Our lack of understanding of the occurrence of metastable monohydrate and the attendant problem of sample reproducibility were major challenges of this study.

Experimental Techniques and Uncertainties

Constant strain rate tests in compression were carried out in our gas deformation apparatus designed for use at cryogenic conditions [*Heard et al.*, 1990]. The apparatus has useful ranges of pressures $0 < P < 600$ MPa, temperatures $77 < T < 300$ K, and strain rates $3.5 \times 10^{-7} < \dot{\varepsilon} < 3.5 \times 10^{-4}$ s^{-1}, and holds a cylindrical test specimen that is typically 25 mm in diameter by 65 mm in length. For the investigation of the NH_3-H_2O system at $x_{NH_3} < 0.33$, most of the experiments were performed in the subsolidus region

TABLE 1. Composition and Run Data for Water + Ammonia Ice Samples

Run (Step)	x_{NH_3}	Bulk Composition*	P, MPa	T, K	ε	$\dot{\varepsilon}$, s^{-1}	σ_u, MPa	σ_{ss}, MPa	Comments
Starting material	0.05	very strong I very weak D very weak M minor G	0.1						
Starting material	0.15	strong I weak D weak M strong G	0.1						
Starting material	0.29	some I strong G	0.1						
219(1)	0.15	55% I, 43% D, 2% M	50	153.0 ± 2.0	0.084	3.79×10^{-5}	74.3	64.5	
219(2)	0.15		50	153.0 ± 2.0	0.117	8.39×10^{-6}		40.0	
219(3)	0.15		50	162.5 ± 2.0	0.154	4.10×10^{-5}		37.0	
219(4)	0.15		50	162.5 ± 2.0	0.218	4.44×10^{-4}		51.7	
219(5)	0.15		50	189.5 ± 2.0	0.226	4.50×10^{-5}		0.5	
219(6)	0.15		50	168.0 ± 2.0	0.312	5.04×10^{-4}		34.9	
219(7)	0.15		50	168.0 ± 2.0	0.352	5.35×10^{-5}		25.3	
220	0.15	65% I, 35% D, ≤1% M	50	171.0 ± 2.0					jacket leak, X ray data only
221	0.15	60% I, 40% D, ≤0.5% M	50	162.0 ± 2.0					jacket leak, X ray data only
222	0.15	55% I, 45% D	50	170.5 ± 2.0					jacket leak, X ray data only
223(1)	0.15	top: 60% I, 18% D, 22% M	50	178.0 ± 2.0	0.019	3.37×10^{-4}		0.6	bottom of sample
223(2)	0.15	bottom: 73% I, 25% M, 2% D	50	176.0 ± 2.0	0.033	3.42×10^{-4}		0.5	more deformed than top;
223(3)	0.15		50	174.0 ± 2.0	0.042	3.45×10^{-4}		0.4	X ray analyses from top
223(4)	0.15		50	172.5 ± 2.0	0.059	3.51×10^{-4}		0.6	and bottom halves of
223(5)	0.15		50	171.5 ± 2.0	0.069	3.55×10^{-4}		0.5	sample
223(6)	0.15		50	169.0 ± 2.0	0.091	3.63×10^{-4}		0.7	
223(7)	0.15		50	167.0 ± 2.0	0.115	3.74×10^{-4}		0.6	
223(8)	0.15		50	159.5 ± 2.0	0.157	3.92×10^{-4}		1.1	
223(9)	0.15		50	151.5 ± 2.0	0.178	4.02×10^{-4}		2.0	
223(10)	0.15		50	142.5 ± 2.0	0.236	4.33×10^{-4}	29.5		fracture; jacket badly ruptured
224(1)	0.05	90% I, 5% D, 5% M	50	168.5 ± 2.0	0.102	3.99×10^{-4}		28.6	not plotted
224(2)	0.05		50	168.5 ± 2.0	0.131	4.13×10^{-5}		23.0	not plotted
224(3)	0.05		50	168.5 ± 2.0	0.156	4.25×10^{-4}		32.5	ended with ductile fault
227	0.01	98–99% I, 1–2% D	50	171.5 ± 2.0					jacket leak, X ray data only
229(1)	0.05		50	168.0 ± 2.0	0.094	3.64×10^{-5}		36.8	
229(2)	0.05		50	168.5 ± 2.0	0.128	3.78×10^{-6}		29.5	
229(3)	0.05		50	149.5 ± 2.0	0.136	3.82×10^{-6}		92.9	
229(4)	0.05		80	149.0 ± 2.0	0.150	3.88×10^{-6}		87.7	
229(5)	0.05		80	158.5 ± 2.0	0.167	3.96×10^{-6}		55.3	
229(6)	0.05		50	158.0 ± 2.0	0.193	4.09×10^{-6}		54.6	
229(7)	0.05		50	168.5 ± 2.0	0.223	4.24×10^{-6}		22.8	
255(1)	0.15	top: 75% I, 25% D	90	145.0 ± 2.0	0.036	3.56×10^{-6}		98.1	sample bulged at bottom;
255(2)	0.15	bottom: 55% I, 45% D	50	144.5 ± 2.0	0.060	3.65×10^{-6}		95.8	X ray analyses from top
255(3)	0.15		50	163.0 ± 2.0	0.092	3.78×10^{-6}		30.6	and bottom halves of
255(4)	0.15		50	168.0 ± 2.0	0.114	3.88×10^{-6}		23.2	sample
255(5)	0.15		50	170.0 ± 2.0	0.143	4.01×10^{-6}		19.2	
255(6)	0.15		50	169.5 ± 2.0	0.175	4.17×10^{-6}		20.2	
255(7)	0.15		50	171.5 ± 2.0	0.186	4.22×10^{-6}		17.4	
256(1)	0.05		90	144.5 ± 2.0	0.060	3.57×10^{-6}		119.0	
256(2)	0.05		100	163.5 ± 2.0	0.087	3.68×10^{-6}		56.0	
256(3)	0.05		50	163.5 ± 2.0	0.107	3.77×10^{-6}		60.6	
256(5)	0.05		50	174.0 ± 2.0	0.118	3.81×10^{-6}		27.4	
256(6)	0.05		50	176.5 ± 2.0	0.126	3.84×10^{-6}		23.3	
256(7)	0.05		50	180.0 ± 2.0	0.138	3.89×10^{-6}		18.1	
258(1)	0.29	15% I, 85% D	50	162.5 ± 2.0	0.032	3.71×10^{-6}		20.9	
258(2)	0.29		50	170.5 ± 2.0	0.053	3.79×10^{-6}		12.7	
258(3)	0.29		50	173.5 ± 2.0	0.077	3.89×10^{-6}		8.9	
258(4)	0.29		50	176.0 ± 2.0	0.087	3.93×10^{-6}		1.3	

TABLE 1. (continued)

Run (Step)	x_{NH_3}	Bulk Composition*	P, MPa	T, K	ε	$\dot{\varepsilon}$, s^{-1}	σ_u, MPa	σ_{ss}, MPa	Comments
260(1)	0.29	9% I, 91% D, ≤1% M	50	132.0 ± 3.0	0.027	3.37×10^{-6}	96.9		fracture, $\phi = 46 \pm 2°$
260(2)	0.29		50	145.0 ± 2.0	0.046	3.44×10^{-6}		91.7	
260(3)	0.29		50	155.0 ± 2.0	0.066	3.51×10^{-6}		45.8	
260(4)	0.29		50	168.0 ± 2.0	0.084	3.58×10^{-6}		13.7	
278	0.05	?? mostly I	50	166.0 ± 2.0					jacket leak, X ray data only
280(1)	0.15	G??	50	170.0 ± 2.0	0.051	3.36×10^{-6}		24.8	poor X ray pattern
280(2)	0.15		50	173.0 ± 2.0	0.079	3.46×10^{-6}		18.7	
280(3)	0.15		50	175.0 ± 2.0	0.130	3.67×10^{-6}		14.9	
280(4)	0.15		50	177.0 ± 2.0	0.149	3.75×10^{-6}		1.0	
283(1)	0.01		50	181.1 ± 1.1	0.041	3.69×10^{-6}		27.3	
283(2)	0.01		50	185.8 ± 1.2	0.069	3.81×10^{-6}		22.9	
283(3)	0.01		50	196.7 ± 1.8	0.112	3.99×10^{-6}		10.1	
283(4)	0.01		50	208.2 ± 1.6	0.142	4.13×10^{-6}		4.8	
283(5)	0.01		50	220.0 ± 2.0	0.189	4.37×10^{-6}		3.7	
284(1)	0.05	90% I, 5% D, 5% M	50	178.4 ± 1.4	0.058	3.44×10^{-6}	30.5	24.6	
284(2)	0.05		50	186.3 ± 1.1	0.080	3.53×10^{-6}		15.2	
284(3)	0.05		50	198.4 ± 1.5	0.110	3.65×10^{-6}		6.5	
284(4)	0.05		50	208.2 ± 1.5	0.140	3.78×10^{-6}		4.0	
284(5)	0.05		50	218.0 ± 2.0	0.130	3.73×10^{-6}		0.1	
287(1)	0.15		50	173.7 ± 1.1	0.042	3.33×10^{-6}		20.6	
287(2)	0.15		50	175.9 ± 0.9	0.096	3.53×10^{-6}		16.2	
287(3)	0.15		50	176.8 ± 1.1	0.136	3.69×10^{-6}		2.0	
294	0.05	??	100	157.5 ± 2.0					jacket leak, X ray data only; poor X ray pattern
295	0.05	92% I, 4% D, 4% M	100	158.2 ± 2.0	0.099	3.61×10^{-6}		58.8	
298(1)	0.15	G??	50	137.5 ± 1.1	0.044	3.42×10^{-7}		115.0	fracture, $\phi \approx 45°$, intersects end cap
298(2)	0.15		50	132.6 ± 1.5	0.048	3.44×10^{-7}	133.0		
300(1)	0.29	9% I, 91% D, ≤1% M	50	138.2 ± 1.2	0.014	3.31×10^{-7}	91.6		fracture, $\phi = 40 \pm 5°$;
300(2)	0.29		50	137.8 ± 1.4	0.063	3.48×10^{-7}		88.5	jacket still intact
300(3)	0.29		50	132.9 ± 1.5	0.093	3.60×10^{-7}	112.6		fracture on different fault plane, $\phi = 37 \pm 2°$
310(1)	0.29	10% I, 90% D, ≤1% M	50	133.5 ± 1.5	0.008	3.50×10^{-7}	85.5		fracture, $\phi = 33 \pm 2°$;
310(2)	0.29		50	138.5 ± 1.8	0.069	3.50×10^{-7}		87.0	jacket still intact
310(3)	0.29		100	138.1 ± 1.2	0.067	3.50×10^{-7}	118.7		failure, on same fault plane
311	0.15 end	60% I, 15% D, 25% M							double sample; hydrostatic pressure only, 30 min
	0.29 end	40% I, 10% D, 50% M							
312	0.15 end	55% I, 44% D, 1% M							double sample; hydrostatic pressure only. 30 min
	0.29 end	12% I, 86% D, 2% M							
316(1)	0.29	15% I, 80% D, 5% M	50	165.7 ± 0.8	0.088	3.83×10^{-4}		35.9	
316(2)	0.29		50	165.7 ± 0.7	0.126	4.00×10^{-5}		22.7	
316(3)	0.29		50	165.8 ± 0.8	0.162	4.17×10^{-6}		14.2	
316(4)	0.29		50	156.9 ± 0.6	0.170	4.21×10^{-6}		33.3	
317(1)	0.29	9% I, 91% D, ≤1% M	50	155.0 ± 0.7	0.031	3.59×10^{-6}		35.0	
317(2)	0.29		50	155.0 ± 0.6	0.078	3.77×10^{-5}		54.0	
317(3)	0.29		50	155.0 ± 0.6	0.088	3.81×10^{-4}	84.2		failure
318(1)	0.29	top end face: 75% I, 23% D,							top end face very icy; melt
318(2)	0.29	2% M							extruded out?
318(3)	0.29	top: 55% I, 44% D, 1–2% M	50	170.9 ± 1.7	0.010	3.46×10^{-4}		1.5	
		bottom: 55% I, 44% D, 1% M	185	170.9 ± 1.7	0.010	0			hydrostatic only, 30 min
			50	170.9 ± 1.7	0.051	3.64×10^{-4}		1.5	unsuccessful X ray search for M

Compositions estimated from XRD on the basis of area under peaks as compared against standards. Composition ranges versus estimated error: 0–3%, ±1; 4–8%, ±2; 9–14%, ±3, 15–24%, ±4; 25–75%, ±5; 76–85%, ±4; 86–91%, ±3; 92–96%, ±2; 97–100%, ±1.

*I, ice I; D, ammonia dihydrate; M, ammonia monohydrate; G, glass.

at $T < 176$ K. The giant icy satellites (Ganymede, Callisto, Titan, and Triton) probably have interior temperatures well above 176 K, and the remaining icy satellites are too small to generate high interior pressures, so we chose relevant testing pressures below 100 MPa. Most of our runs were conducted at 50 MPa, and we varied pressure mainly to inhibit fracturing rather than to measure intrinsic dependence of flow on pressure.

As with any new and unknown material, our experimental and analytical techniques evolved with experience. Particularly important to note in this study is that our ability to avoid systematic problems improved markedly over the course of this study, so early data lack the quality of later data. This distinction generally cannot be quantified with error bars, but discussion in the text is provided in situations where the uncertainty is relevant. We suspect systematic errors from two sources: perforation of the indium jacket and the presence of nonequilibrium phases, in particular, monohydrate. Jacket leaks in pure ice samples are almost always manifested by pronounced sample weakness, but in ammonia-water samples, especially near the peritectic, we discovered that minute perforations in the jacket are not always accompanied by large anomalies in the load displacement record. On the other hand, small strength anomalies are not always the result of jacket leaks, so it follows that some data may have been subtly affected by undetected jacket leaks. We eventually removed this uncertainty by building a sample assembly that vents to room pressure, thus preventing any buildup of pressure inside the sample jacket and concomitant loss of effective confinement. All runs with number 297 or greater have this added certainty.

Regarding the presence of nonequilibrium phases, we have already noted the existence of monohydrate in some samples. There is evidence in our experiments that monohydrate is substantially weaker than dihydrate, so we are left with an uncertainty analogous to that introduced by the possibility of jacket leaks: most of the samples were probably chemically equilibrated assemblages of water ice and dihydrate, but nonequilibrium phases may have been present in some of the few samples that exhibited anomalous stress-strain behavior.

EXPERIMENTAL RESULTS

Samples of $x_{NH_3} = 0.01$, 0.05, 0.15, and 0.295 were deformed at temperatures from $133 < T < 220$ K, strain rates $3.42 \times 10^{-7} < \dot{\varepsilon} < 5.04 \times 10^{-4}$ s^{-1}, and pressures $50 < P < 100$ MPa. The sample responses ranged from brittle to ductile and include deformation under conditions of partial melting. Portions of two stress-strain records are shown in Figure 3 to illustrate the salient features of the experiments. A piston moving at a constant displacement rate $\dot{u}$ (converted to strain rate $\dot{\varepsilon}$ by normalizing by the instantaneous sample length) first loads a sample elastically (the initial, linear portions of the curves). Differential stress is calculated in the usual way by dividing the measured quantity, force on the sample, by the instantaneous base area of the sample, the latter calculated from the known amount of shortening of the sample and an assumed model of a uniformly straining fixed volume of material. As the sample begins to yield plastically, the curve begins to deflect from the elastic curve. In the case of the $T = 134$ K run illustrated in Figure 3, sudden failure occurred as the sample began to yield, indicated by the downward pointing arrow at the ultimate level of differential stress σ_u that the sample withstood. For ductile deformation, illustrated by the $T = 155$ K run in Figure 3, we define ultimate strength σ_u as the point where the stress-displacement curve reaches a maximum. Previously undeformed pure water ice invariably loses strength following σ_u but eventually (after permanent strains of 5–10%) attains a state where differential stress is independent of displacement. We define the differential stress in this "steady state" σ_{ss}. For virtually all of our ammonia + water samples, $\sigma_u \approx \sigma_{ss}$; hence σ_u is labeled parenthetically in Figure 3, and notation of σ_u for such samples is usually not given in Table 1. Most runs are stepped in temperature and/or displacement rate in order to gain additional data points; that is, once σ_{ss} is achieved and there is no suggestion that it will change with further strain, we withdraw the piston to unload the sample, change run conditions, then advance the piston again once temperatures and pressures have reequilibrated.

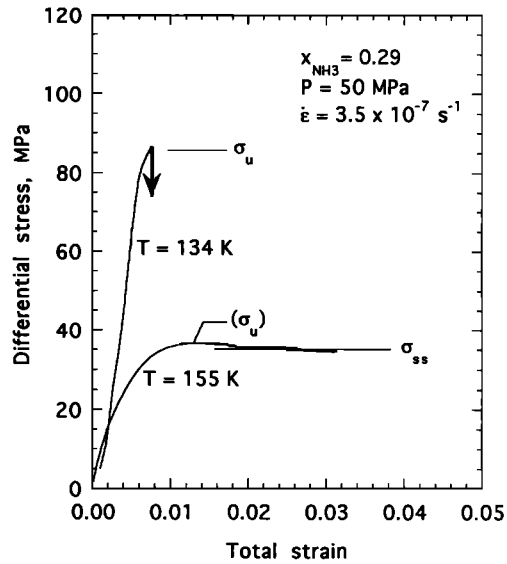

Fig. 3. Portions of the stress-strain record for runs at $T = 134$ K (run 310) and 155 K (run 317) illustrating some typical features of the mechanical response of ices in the NH_3-H_2O system. Stress and strain are calculated from measured force on the sample and measured shortening of the sample. Total strain includes elastic plus inelastic permanent strain. After deforming mostly elastically, the $T = 134$ K sample began slow inelastic deformation (evidenced by the slight curvature near the top of the trace), then failed suddenly at the ultimate stress level, labeled σ_u. The 155 K sample showed ductile deformation after the initial elastic loading, reaching a maximum stress (also labeled σ_u) and then an approximately steady level of stress, labeled σ_{ss}. The label σ_u is shown in parentheses because in most NH_3-H_2O samples σ_u differs little from σ_{ss} and is usually not noted in Table 1. In contrast, σ_u is invariably 25% or more higher than σ_{ss} for pure water ice samples (see, e.g., Table 2).

Strength data for samples in the ammonia-water system are summarized and compared with those of pure water ice in Figure 4 and in selected subsets of the data in Figures 5–9, with additional information on faulting and microstructure in Figures 10 and 11. The "analysis" section that follows provides further detailed descriptions and analysis that the reader, depending on motivation, may choose to skip in favor of the data synthesis and discussion of planetary applications that follow. The results of this study can be summarized as follows:

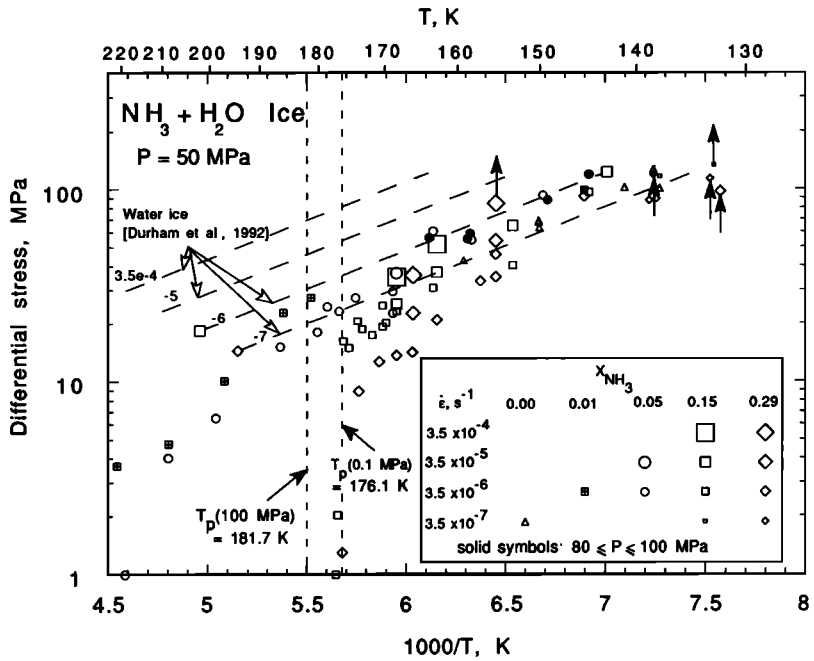

Fig. 4. Arrhenius plot of all data listed in Tables 1 and 2 (except from runs 224 and 318, see text), showing the steady state ductile strength of solids and liquid/solid mixtures in the NH_3-H_2O system. Differing chemical compositions are indicated by shapes of the symbols and strain rates by sizes of the symbols. Solid symbols indicate run pressures of 80 to 100 MPa; open symbols indicate run pressures of 50 MPa. There does not seem to be any pronounced strengthening or weakening caused by a moderate pressure increase. Arrows pointing upward indicate points of sudden failure; presumably, ductile strength would be higher if failure could be suppressed. Points are shown without error bars to avoid additional clutter. The long-dashed lines represent the low-temperature-regime flow law for pure water ice [*Durham et al.*, 1992] at the strain rates shown. Strain rates here and in subsequent figures are labeled simply with the appropriate power of 10. The vertical dashed lines indicate the peritectic temperatures at 0.1 and (estimated at) 100 MPa.

1. Samples of composition $x_{NH_3} = 0.295$ (mole fraction dihydrate $x_D = 0.90$) are substantially weaker at $T > 145$ K than pure water ice at the same conditions and show a greater temperature sensitivity of strength (Figure 5). At $T <$ 140 K dihydrate is as strong or stronger than water ice (Figure 9).

2. At temperatures just below the peritectic, steady state strengths of two-phase water ice-dihydrate alloys increase progressively as the volume percent water ice increases (Figure 6).

3. Samples that have abundant dihydrate ($x_{NH_3} \geq 0.15$, $x_D \geq 0.45$) have negligible strength at temperatures above 176 K (Figure 6). This confirms the general expectation that the narrow melting interval for dihydrate would cause a sudden weakening at those temperatures for alloys with substantial volume fractions of dihydrate.

4. Water ice + dihydrate alloys with $x_{NH_3} = 0.01$ and 0.05 ($x_D = 0.03$ and 0.15), while having subsolidus strengths that are closer to that of water ice, show significant strength at temperatures above the dihydrate-monohydrate eutectic at 175.4 K.

5. At high differential stresses, water ice + dihydrate alloys fail by a mechanism that resembles a shear instability in pure water ice caused by the ice I → ice II phase transformation (Figure 10). The faulting even occurs in samples of $x_D = 0.90$.

ANALYSIS

The results of the experiments on solids and partial melts in the NH_3-H_2O system do not lend themselves to concise analysis. This section is provided for readers seeking a detailed understanding of the mechanical and thermodynamic behavior of materials in this system. The major points of the paper will not be overlooked by those skipping this section and proceeding to the next.

Subsolidus ductile flow. Results for samples of fixed composition $x_{NH_3} = 0.295$ ($x_D = 0.90$) are plotted in Figure 5. For $145 < T < 176$ K, this alloy follows a flow law of the form followed by water ice and many other solids:

$$\dot{\varepsilon} = A\sigma_{ss}^{n} e^{-Q/RT} \tag{1}$$

where A, the stress exponent n, and the activation energy Q are material constants and R is the gas constant 8.31 J/K mol. A least squares fit to the data at $\dot{\varepsilon} = 3.5 \times 10^{-6}$ s^{-1} in Figure 5 constrains the value of Q/n to 17.7 ± 1.3 kJ/mol (error covers all scatter). The value of n, inversely proportional to the (log) vertical distance between lines of constant $\dot{\varepsilon}$ in Figure 5, is $n = 5.8 \pm 1$. Our best determination of the flow law of the $x_D = 0.90$ alloy, indicated by the lines in Figure 5 is thus (1) with the constants

$$A = 10^{19.8}\ \text{MPa}^{-n}\ \text{s}^{-1}$$

$$n = 5.8 \tag{2}$$

$$Q = 102.3\ \text{kJ/mol}$$

For now this flow law will serve as an approximation of the flow of pure dihydrate. A small correction based on the flow

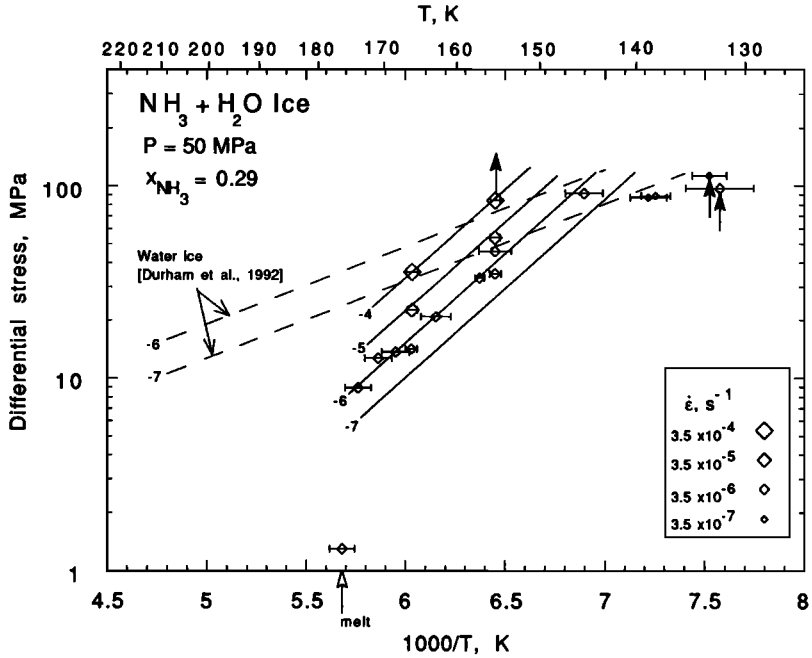

Fig. 5. Flow and fracture in nearly pure dihydrate, represented here by all data from the x_{NH_3} = 0.295 ice + dihydrate alloy. The horizontal error bars in this and following figures are from Table 1 and include uncertainty as well as variation over time. Flow laws for ice at the two lowest strain rates are shown by the dashed lines.

results for the other water ice + dihydrate alloys will be applied later to give the flow law for truly pure dihydrate.

The results for other ice + dihydrate alloys are shown in Figures 6–8. Figure 6 compares the strengths of various compositions at a fixed strain rate of $\dot{\varepsilon} = 3.5 \times 10^{-6}$ s^{-1}. Flow laws for binary mixtures should converge at the temperature where end member strengths are identical [*Tullis et al.*, 1991], and it appears in Figure 6 that the three best resolved flow laws, for $x_{NH_3} = 0$ (i.e., pure water ice), 0.15, and 0.295, converge at the same point near T = 140 to 145 K. The flow law for x_{NH_3} = 0.05 misses this convergence point by a considerable margin. We note, however, that there are only six data points for this mixture below 176 K, and they are badly scattered. X ray measurements of the x_{NH_3} = 0.05 samples show the most consistent appearance of ammonia monohydrate, which may have weakened some of

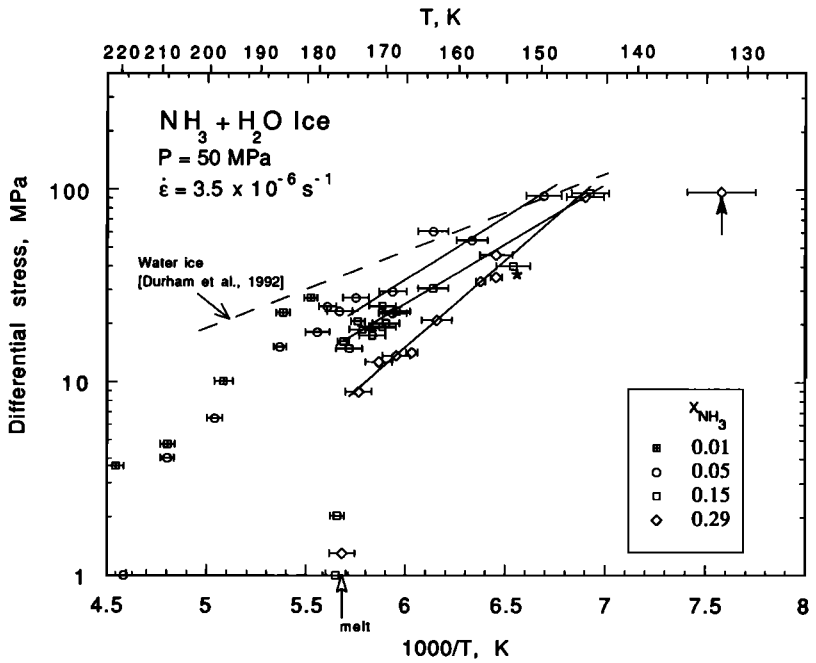

Fig. 6. Flow of ices at fixed strain rate, 3.5×10^{-6} s^{-1} for different compositions in the NH_3-H_2O system. Solid lines are least squares fits to subsolidus data. The x_{NH_3} = 0.15 point labeled with an asterisk was not used in the fit because this and other points taken from that run (run 219; see also text and Figure 7) were anomalously weak.

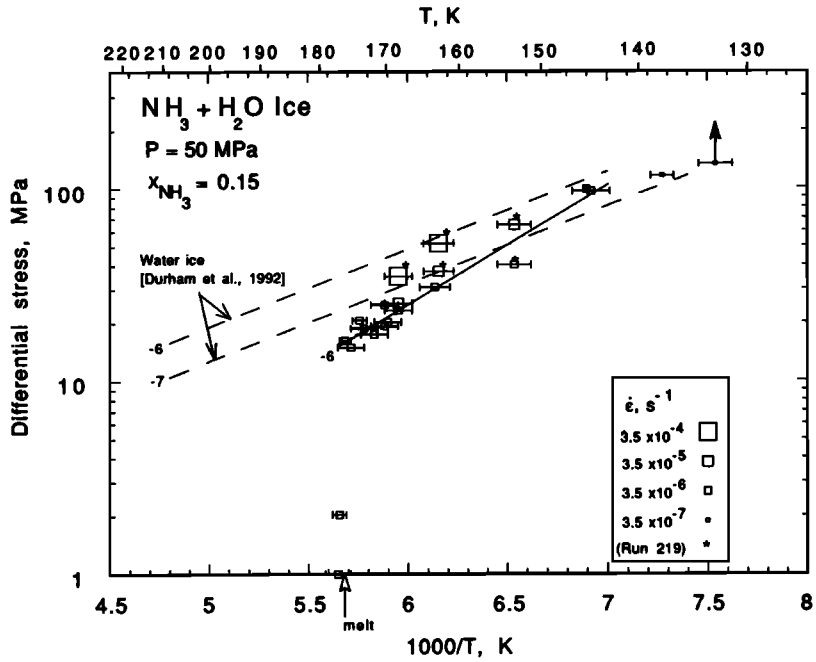

Fig. 7. Measurements of the flow of the ice + dihydrate alloy $x_{NH_3} = 0.15$ (mole fraction dihydrate $x_D = 0.45$). Solid line is least squares exponential fit to subsolidus points of $\dot{\varepsilon} = 3.5 \times 10^{-6}$ s^{-1}, the same shown in Figure 6. The five points labeled with an asterisk were from run 219 (see text).

the samples deformed at higher temperatures, as discussed below.

Results for all strain rates for ice + dihydrate alloys $x_{NH_3} = 0.15$ and 0.05 ($x_D = 0.45$ and 0.15, respectively) are shown in Figures 7 and 8, respectively. The bulk of the measurements for both compositions were made at $\dot{\varepsilon} = 3.5 \times 10^{-6}$ s^{-1}, so in fitting the data to (1), the slope Q/n of the lines of constant strain rate is well constrained, but the value of n is poorly constrained. The few strain-rate-stepping results for these alloys put n somewhere in the range of 5–10, consistent with the values for dihydrate (5.8) and for water ice (5.6).

Is dihydrate stronger than water ice at $T < 145$ K? Above 145 K, dihydrate is softer than water ice. The stress exponent n for dihydrate and ice are comparable, but the strength of dihydrate is much more temperature-sensitive than that of ice. Thus the strength contrast between dihydrate and ice at a given strain rate changes considerably

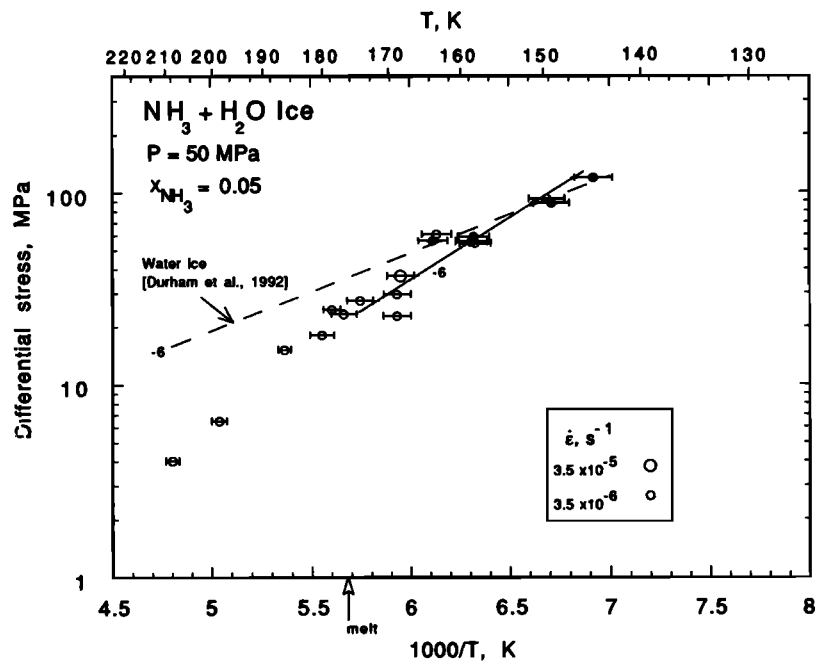

Fig. 8. Measurements of the flow of the ice + dihydrate alloy $x_{NH_3} = 0.05$ ($x_D = 0.15$). Solid points are for $P > 50$ MPa. Solid line is least squares fit to subsolidus points of $\dot{\varepsilon} = 3.5 \times 10^{-6}$ s^{-1} and $P = 50$ MPa.

TABLE 2. Run Data for Pure Water Ice Samples

Run (Step)	P, MPa	T, K	ε	$\dot{\varepsilon}$, s^{-1}	σ_u, MPa	σ_{ss}, MPa	Comments
297(1)	50	158.5 ± 2.0	0.079	3.57×10^{-7}	65.2	(45.6)	strength still falling
297(2)	50	149.9 ± 1.3	0.109	3.69×10^{-7}		62.8	
297(3)	50	137.5 ± 1.4	0.127	3.77×10^{-7}		100.5	
297(4)	50	159.0 ± 1.3	0.149	3.86×10^{-7}		42.4	
299(1)	50	138.1 ± 2.3	0.055	3.50×10^{-7}*		126.0	
299(2)	50	138.6 ± 1.4	0.072	3.49×10^{-7}	124.2		fracture
315(1)	50	150.0 ± 1.1	0.106	3.67×10^{-7}	96.3	67.0	
315(2)	80	150.0 ± 1.1	0.120	3.73×10^{-7}		68.3	
315(3)	50	140.9 ± 1.5	0.158	3.90×10^{-7}	101.2	101.2	fracture during apparent s.s.

*On/off, not yet s.s.

with temperature, from a factor of about 5 just below the solidus (which translates to a factor of $5^n \approx 10^4$ in effective viscosity) to almost no difference near 145 K. Because the planetological implications of strong dihydrate are so important, we replaced the closed sample assembly with a vented one to allow reliable testing at a lower strain rate, namely, 3.5×10^{-7} s^{-1}, thus allowing us to achieve ductility at lower temperatures than previously attainable.

We then carried out a series of six runs on water ice and on our $x_D = 0.90$ ($x_{NH_3} = 0.295$) samples. Each run lasted about a week, and all were carried out over a 5-month period to keep any effect of sensor drift (of the thermocouples in particular) to a minimum. Redundant thermocouples retained consistent readings throughout these tests, so the greatest contribution to the error bars is real temperature fluctuations, rather than uncertainty.

The results for the water ice samples are listed in Table 2, and the combined measurements for both pure and mixed-phase samples are plotted in Figure 9. The order of magnitude decrease in strain rate has pushed our limit of ductility to about 138 K, where as can be seen in Figure 9, water ice and dihydrate have comparable strengths. Note the following details in Figure 9: (1) the strength of water ice corresponds closely to the extrapolation of the flow law determined from tests at higher temperatures [*Durham et al.*, 1992] i.e., the dashed line in Figure 9; (2) the strength of dihydrate lies below the extension of the $145 < T < 176$ K dihydrate flow law, i.e., the solid line in Figure 9, suggesting a change occurs in the dominant mechanism of flow below 145 K; (3) the colder dihydrate samples tended to fail by faulting before achieving full ductility (see also the following section); and (4) samples of $x_{NH_3} = 0.15$ and 0.295 have comparable strengths at $T \approx 138$ K. Thus the ductile strength of water ice probably does lie along the dashed line in Figure 9, but the measured failure strength of dihydrate at 132 K is at best a lower bound on its ductile strength. We

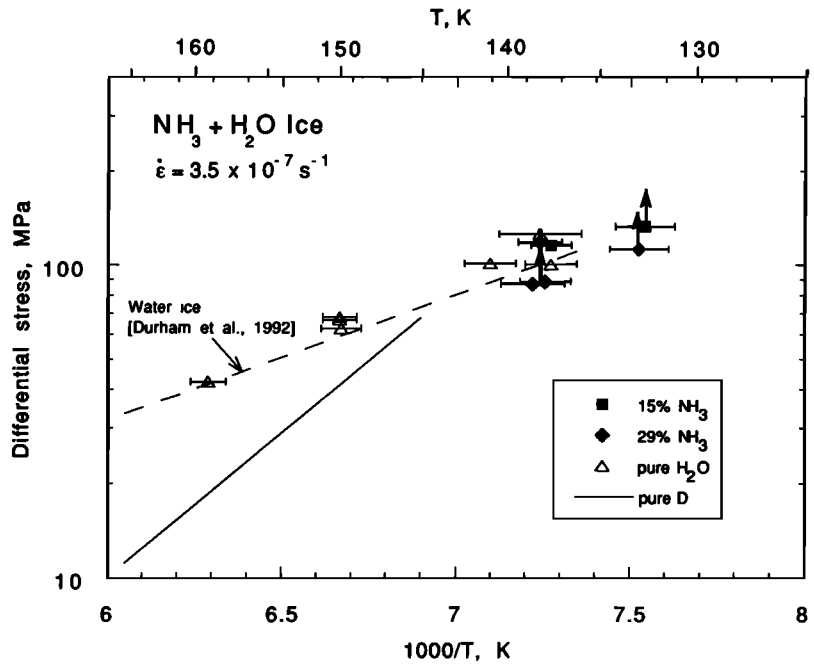

Fig. 9. Comparison of the flow and fracture behavior of pure water ice and ice + dihydrate alloys at low temperatures. The solid line is the least squares fit to all the $x_{NH_3} = 0.295$ data (equation (2) and Figure 5).

conclude that at $T < 140$ K, dihydrate is as strong or stronger than water ice at laboratory strain rates.

Ammonia monohydrate. Ammonia monohydrate should not appear as an equilibrium phase based on the phase diagram (Figure 1) and the bulk composition of our samples. Even if melt fractionation or other differentiation of the samples had occurred, it is still difficult to explain significant amounts of monohydrate: the first liquid to appear in our system remains slightly more NH_3-rich than pure dihydrate up to about 179 K, so a small amount of monohydrate should form if this liquid refroze without reequilibrating with the parent material. However, relatively large amounts of monohydrate have appeared in some of the samples, and there are systematic trends to its appearance (Table 1): (1) It appeared in all three of the $x_{NH_3} = 0.05$ samples that were examined and that produced good X ray patterns. For all three the monohydrate/dihydrate ratio was about 1.0 (Table 1). (2) It appeared strongly in $x_{NH_3} = 0.15$ sample 223, one of the two samples heated to just above the 176-K peritectic before being cooled, and it appeared prominently in sample 311. That sample was a hydrostatically annealed double sample of $x_{NH_3} = 0.15$ and 0.295, which was handled with less care than samples intended for deformation and which was taken well above 176 K (5 K or more) before its 143-K anneal. The only other deformation sample heated above the peritectic was sample 219, but it was heated not slightly above but well above (to 189 K), and monohydrate appeared only weakly.

Strength and the appearance of monohydrate may be correlated. We have already pointed out that the best fit to the subsolidus results for $x_{NH_3} = 0.05$ seems weaker than expected based on measurements of other ice + dihydrate alloys. Deep supercooling of the melt is known to occur [*Kargel et al.*, 1991, and references therein] and may explain the near zero strength of sample 223. Sample 318, which also showed essentially zero strength at 170 K, arrived at its run temperature from 77 K but showed no X ray evidence for monohydrate (despite a rather intensive search, Table 1). *Van Kasteren* [1973] observed that if an NH_3-H_2O mixture of $x_{NH_3} = 0.095$ is frozen rapidly and held at low temperature for 150 hours, it melts at 171 K. (Held for shorter times, it shows melting reactions over a range from 171 to 176 K.) Van Kasteren also found that a mixture of $x_{NH_3} = 0.27$ treated in the same way invariably melts at 176.2 K. Note that we never saw premature liquid in our samples of $x_{NH_3} = 0.295$, and usually detected only faint monohydrate in those samples (Table 1). Further investigation of the strength of monohydrate is clearly called for. The possibility exists that the processes we observe may produce monohydrate at low pressures in the solar system. Monohydrate may also exist in substantial quantity in the deep interiors of very large moons: diamond cell experiments by *Cynn et al.* [1989] suggest that monohydrate, not dihydrate, is the phase in equilibrium with water ice polymorphs above approximately 2 GPa.

The role of pressure in the kinetics of phase transformation is unclear. Densities near the peritectic are about 0.93 for the liquid, 0.96 for monohydrate, and 0.98 Mg/m^3 for dihydrate [*Croft et al.*, 1988]. If the glass that appears prominently in the as-molded starting material (Figure 2*b*) has the same density as the liquid, then pressurization should favor its crystallization, which, as noted earlier, seems to have occurred in nearly every sample (Table 1). However, pressurization of the supercooled liquid did not seem to have induced crystallization in samples 223 or 318. We pressurized sample 318 to 180 MPa at 171 K but succeeded only in extruding sample material out the vented force gauge. *Hogenboom and Kargel* [1990] did find an effect of pressure in recrystallization of melted dihydrate when one did not venture too far in temperature and time from the point of melting: above 100 MPa, monohydrate recrystallizes from the melt; below 100 MPa the liquid simply supercools.

Rheology of partial melts. The peritectic melting of dihydrate at 176.1 K (Figure 1) appears prominently in the rheology of dihydrate-rich samples $x_{NH_3} = 0.15$ and 0.295 (Figure 4). The transition is sharp: at $T < 176$ K, pure dihydrate follows the dihydrate flow law given above (equations (1) and (2)); at $T > 176$ K, it has virtually no strength. The transition is not sharp in the samples of lower NH_3 concentration. This is not surprising in the $x_{NH_3} = 0.01$ samples, which have only a 3% melt volume. However, in the $x_{NH_3} = 0.05$ samples, which become about 15% molten at the peritectic if they are water ice + dihydrate, the lack of a transition is unexpected. If, on the other hand, the $x_{NH_3} = 0.05$ samples have a significant monohydrate component that is relatively weak below 176 K (or that even melts at 171 K), the change in rheological properties at 176 K might not be as sharp.

Two samples were purposely taken well above 176 K in a cursory exploration of the rheological effects of lower amounts of partial melts in the NH_3-H_2O system. Two samples, one each of $x_{NH_3} = 0.01$ and $x_{NH_3} = 0.05$, were deformed in matching temperature steps where the amount of imposed strain was also matched step for step. They had relatively high strengths just above the peritectic, evidently reflecting the low melt fractions (3% and 15%, respectively). With increasing temperatures, however, strengths of both eventually fell well below that of water ice, even though melt fractions increased only slightly (to 4% and 20%, respectively, at 220 K). Weakening does not correlate in a simple way with melt fraction. For example, interpolating the points in Figure 6, a sample with 4% melt at 208 K (an $x_{NH_3} = 0.01$ sample) has about the same strength as a sample with 17% melt ($x_{NH_3} = 0.05$) a few degrees cooler. Note also that at 220 K the $x_{NH_3} = 0.05$ sample had essentially lost all its strength, but the $x_{NH_3} = 0.01$ sample had ceased its dramatic drop in strength, giving the trend of the data a sigmoidal shape in Figure 4. The imposed strain in the $x_{NH_3} = 0.01$ sample by this point was 0.19, so melt segregation to the sides of the sample, leaving a solid framework of ice to support the load, is a distinct possibility. We did not do a textural analysis of this sample, so this remains a conjecture.

Generalization of these results to the rheology of partial melts in the NH_3-H_2O system is inappropriate because the approximately 0.25-mm grain size in our samples was probably too large to have allowed textural equilibration of the solid and liquid phases over the short duration of the experiments. *Cooper and Kohlstedt* [1986] have emphasized the importance of achieving textural equilibration in partially molten test specimens if results are to be extrapolated to geological strain rates, which are typically several orders of magnitude slower than convenient laboratory strain rates. Solution-precipitation processes [*Cooper and Kohlstedt*, 1986; *Stevenson and Lunine*, 1986] can be expected to dominate the deformation of partial melts, where it can be shown that required equilibration time is of the order of the

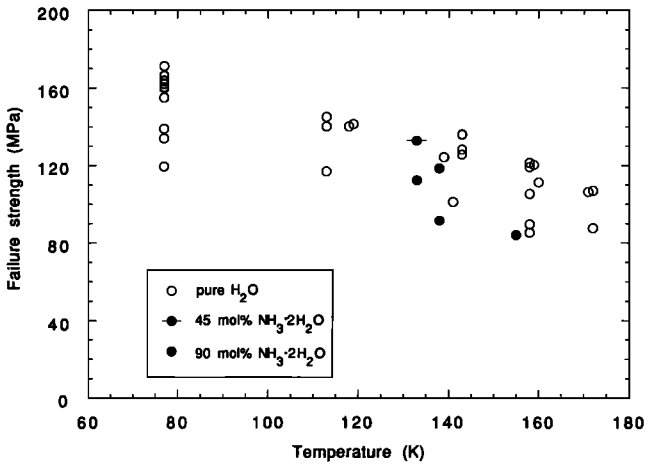

Fig. 10. Differential stress level at failure (i.e., failure or ultimate strength σ_u) as a function of temperature for all water ice (open figures) and water ice + dihydrate (solid figures) samples that have exhibited a shear instability in our apparatus. Runs for which confining pressure was <50 MPa are not shown; otherwise, data are shown without regard to strain rate or pressure, which have only a small effect on failure strength in this regime. External causes for the scatter are suspected (see text). The closed figures (Table 1) and two of the open figures (Table 2) come from this study. All other measurements have been published previously [*Durham et al.*, 1983; *Kirby et al.*, 1991].

time required for the slowest moving species to diffuse the length of one grain boundary [*Cooper and Kohlstedt*, 1986].

Shear instability in dihydrate-bearing samples. Several runs on x_{NH_3} = 0.15 and 0.295 samples resulted in sudden failure on single fault planes that were oriented at unusually high angles to the compression direction (40°–46°). This behavior is restricted to experiments at $T \leq 155$ K at 50 MPa confining pressure and mostly at the lowest strain rates. Our understanding of this phenomenon suffers from the small number of runs and the large scatter in measured strengths. The shear instability seems to be a high-stress phenomenon, but note, for example, several instances in Table 1 where ductility in some samples was maintained at stress levels well in excess of the levels where other samples faulted. All of the observed faults intersected the end caps. We suspect that misalignment of the sample ends, possibly associated with the pressure-induced devitrification process discussed earlier, may play a role in this reproducibility problem. Nonetheless, the high faulting angle and the roughly comparable faulting strength to that of the shear instability in pure ice (Figure 10) mentioned earlier invite comparison of the two phenomena.

Durham et al. [1983] and *Kirby et al.* [1985] noted that faulting strength of pure ice in this regime is independent of confining pressure and that the faulting angle is close to 45°, both features being inconsistent with ordinary brittle fracture. *Kirby* [1987] pointed out that anomalous faulting occurs in pure ice I samples only when the experimental conditions place them metastably in the field of ice II and at temperatures low enough that the rate of the ice I → II reaction is sluggish. *Kirby et al.* [1991] confirmed that ice II occurred in all samples examined that exhibited this shear instability, and so termed the phenomenon transformational faulting. They also noted that ice samples that faulted in this manner always exhibited a distribution of ice II microinclusions, some of which were in inclined arrays, suggesting sites of transformational fault nucleation. In the present study, samples in the ammonia-water system that faulted at 50 MPa did not show X ray evidence for any new phases that were not present before deformation. Our minimum level of detection of ice II is a few percent, so we cannot exclude the possibility that as much as 20% of the roughly 10 vol % ice I in x_{NH_3} = 0.295 samples transformed to ice II.

In this comparison, we have not demonstrated that the faulting instability in samples in the ammonia-water system is independent of pressure as it is in pure ice, so the observed faulting could be ordinary fracture with an unusually high faulting angle. Alternatively, transformational faulting or similar shear instability may operate when only 10% ice I is present. Additional experiments are clearly needed in order to resolve these questions.

Microstructures in ice + dihydrate alloys. The formation of dihydrate from the liquid or amorphous solid results in a densification of about −1.8%, a volume change that should produce surface depressions where dihydrate grows at the sample surface. These depressions are replicated on the inner surface of the indium jackets as high-standing relief. Inspection of those jackets showed platelike features raised above the background surface in samples that display strong dihydrate X ray peaks along with water ice peaks (Figures 11*b* and 11*c*). These features are usually absent from the x_{NH_3} = 0.295 samples that are mostly dihydrate and from pure ice samples deformed in this same pressure and temperature range, confirming that they probably represent dihydrate on the sample surface. Moreover, the lamellar features are weakly developed or absent in the x_{NH_3} = 0.05 samples that have mixed dihydrate and monohydrate patterns. Although the lamellar features show a wide range of orientations with respect to the compression direction in samples deformed to moderate strains, samples deformed to large strains (Figure 11*c*) had dihydrate lamellae that form a foliated texture nearly perpendicular to the compression direction. The foregoing microscopic observations, together with our finding that dihydrate is weaker than ice at most temperatures (Figure 5), suggests that plastic deformation of dihydrate contributes to the surface relief seen in Figures 11*b* and 11*c* and intracrystalline slip in dihydrate lamellae is partly responsible for the rotation of lamellae shown by samples like that shown in Figure 11*b*.

SUBSOLIDUS FLOW LAW FOR THE NH_3-H_2O SYSTEM

The analysis by *Tullis et al.* [1991] provides a basis for deriving a general flow law for mixed solids in the NH_3-H_2O system from the measurements in this study. The derivation is somewhat complex and is model-based, but simplicity is introduced by the result that dihydrate follows a single flow law over a wide temperature range (Figure 5), and the x_{NH_3} = 0.15 mixture of x_D = 0.45 behaves equally well and lies between the flow of pure ice and (almost) pure dihydrate (Figure 6). Further assurance of simplicity comes from the few results, once rationalized for the presence of monohydrate, of the x_{NH_3} = 0.05 mixture.

Tullis et al. [1991] modeled the flow of two-phase solid mixtures as a function of end-member flow laws and volume fraction of each phase. Flow of mixtures is of course dependent on texture (how the two phases are arranged geometrically), and Tullis et al. have shown that reasonable

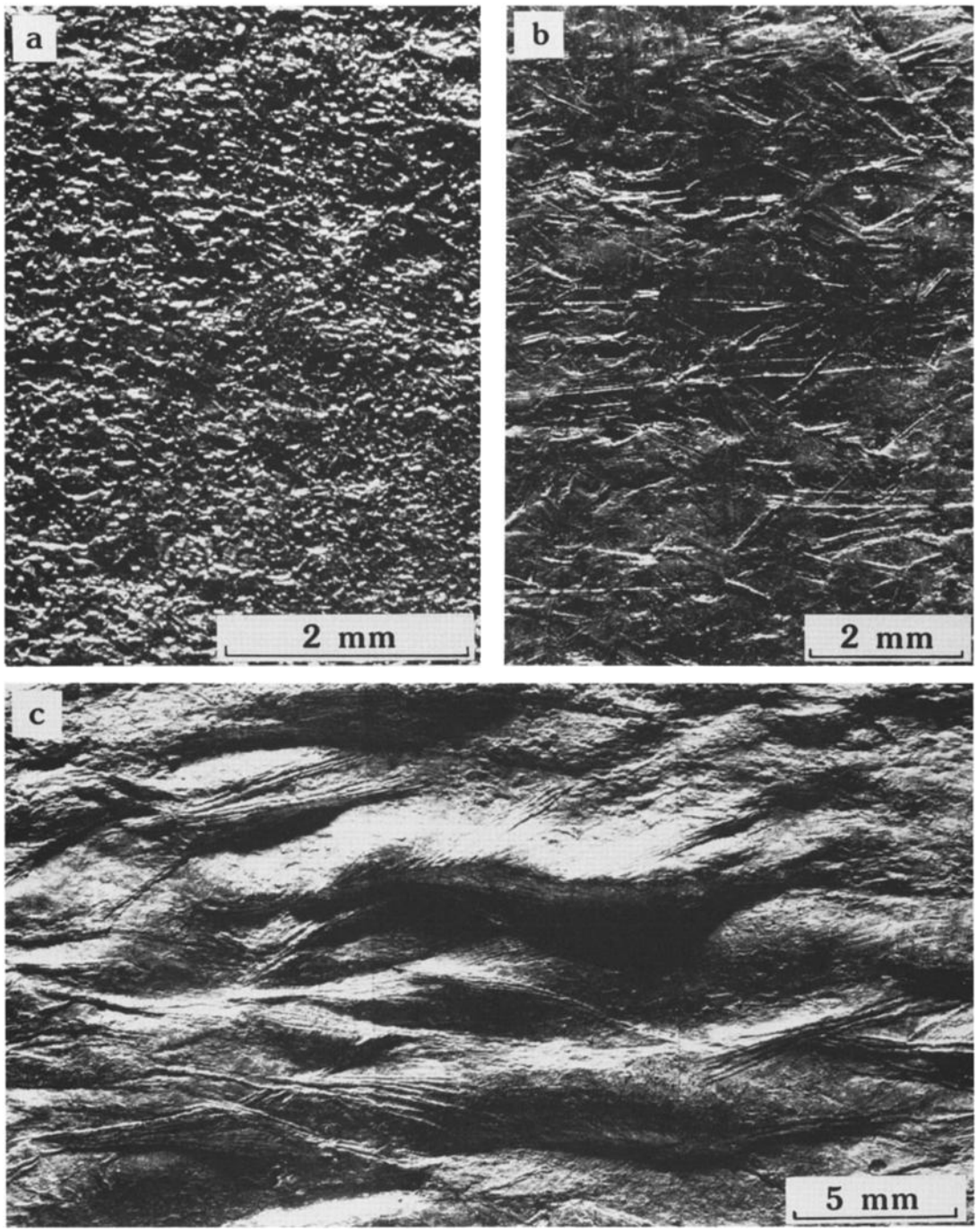

Fig. 11. Sample surfaces replicated by the encapsulating indium jackets for (*a*) run 295, $x_{NH_3} = 0.05$, $\varepsilon = 0.099$; (*b*) run 280, $x_{NH_3} = 0.15$, $\varepsilon = 0.149$; and (*c*) run 219, $x_{NH_3} = 0.15$, $\varepsilon = 0.352$. Dihydrate stands out in relief as raised lamellar features. Textures in Figures 11*a* and 11*b* are representative of deformed samples of $x_{NH_3} = 0.05$ and 0.15. Run 219 (Figure 11*c*) was partially melted and is the only sample to show such a coarsely recrystallized and foliated texture.

upper and lower bounds for extremes of texture are a uniform strain condition, where both phases strain at exactly the same rate, and a uniform stress condition, where both phases experience the same differential stress. Applying their relationships to our water ice + dihydrate alloys and taking the $x_{NH_3} = 0.295$ flow law as an approximation for that of the dihydrate end-member, we show in Figure 12 these bounds for $\dot{\varepsilon} = 3.5 \times 10^{-6}$ s^{-1} at two temperatures. Plotting our actual measurements in the coordinates of Figure 12 (open symbols, labeled "orig") shows that the flow of aggregates of water ice and dihydrate lies reasonably [*Tullis et al.*, 1991] between the uniform stress and uniform strain rate models. More importantly, the plot provides a model for estimating the strength of pure dihydrate and hence the strength of any water ice + dihydrate alloy. The model, a smooth curve through the original data but constrained to start and end at the corners of the plot, indicates about a 5% difference between the strength of pure dihydrate and of $x_{NH_3} = 0.295$ solids at 167 K and 3.5×10^{-6} s^{-1}. The solid symbols in Figure 12 ("corr") are adjusted accord-

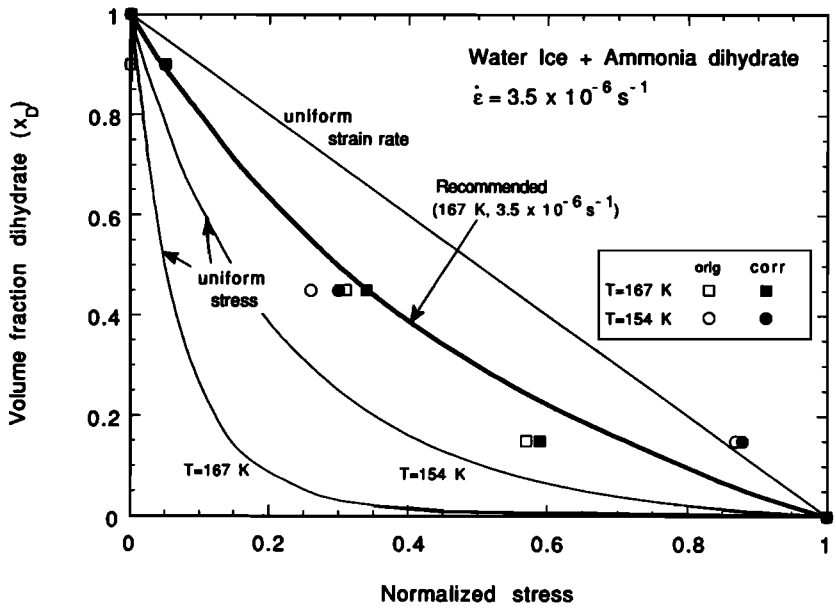

Fig. 12. Strength of solid water ice + dihydrate alloys at fixed temperature and strain rate as a function of composition, plotted in the manner of *Tullis et al.* [1991]. The zero value of normalized stress is the strength of the weaker end-member (dihydrate) at the temperature in question (here we show curves for 154 and 167 K); the value 1.0 is the strength of the stronger end-member (water ice). The bolder curve is our best estimate for the flow of all ice + dihydrate alloys at 167 K and $3.5 \times 10^{-6}\ s^{-1}$.

ingly. Constraining the model at 167 K to pass through the solid square at $x_D = 0.45$ (which is based on the well-resolved measurement from Figure 7) then gives the bold curve in Figure 12, which is our best estimate for the flow at this strain rate and temperature for all alloys. The results for all temperatures and for several representative mixtures are shown in Figure 13. The equiviscous point is at $T = 143$ K.

Strain-rate dependence is also model-dependent. A geometric averaging scheme suggested by *Tullis et al.* [1991], to be used where measurements are absent, is

$$\log n_a = x_D \log n_D + (1 - x_D) \log n_I \qquad (3)$$

where the subscripts a, D, and I indicate the aggregate, dihydrate, and water ice. There is little error in making this estimate since n_D (≈ 5.80, based on $x_D = 0.90$) and n_I ($= 5.60$) are so similar. We summarize our model in Table 3 with sets of flow law constants for the full range of dihydrate mole fractions.

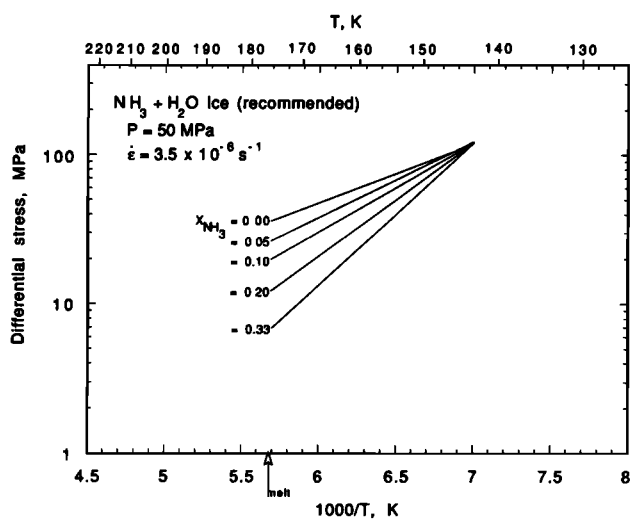

Fig. 13. Flow laws calculated from our application of the model of *Tullis et al.* [1991] for a spectrum of ice + dihydrate alloys over the entire temperature range for which its validity has been experimentally established (see text for explanation). Given the stress exponent n (which varies only slightly from 5.6 for $x_D = 0$ to 5.81 for $x_D = 1.0$ (equation (3)), the strength of an alloy can be determined at any temperature and strain rate.

APPLICATION TO THE ICY MOONS

Application of the results of the present study depend critically on the hypotheses mentioned in the introduction for the formation of molecular species like ammonia in the outer solar system and how they differentiate and concentrate in the course of planetary evolution. There is ample visual evidence, for example, to support pre-Voyager expectations of the presence of NH_3 ices on low-density moons of the outer solar system [*Lewis*, 1971], from extensive resurfacing suggestive of voluminous low-temperature liquids

TABLE 3. Flow Constants for Water Ice and Ammonia Dihydrate Alloys at $P = 50$ MPa, $143 < T < 176$ K

Mole Fraction Dihydrate x_D	$\log A_a$, $MPa^{-n_a}\ s^{-1}$	n_a	Q_a, kJ/mol
1.0	21.55	5.81	107.5
0.6	13.08	5.73	83.6
0.3	6.45	5.66	65.1
0.15	2.56	5.63	54.1
0	−1.40	5.60	43.0

$\dot{\varepsilon} = A_a\ \sigma_{ss}^{n_a}\ e^{-Q_a/RT}$.

[e.g., *Squyres et al.*, 1983] to viscous surface extrusions [*Jankowski and Squyres*, 1988; *Schenk*, 1991] to tectonic activity at temperatures probably too cold to be explained by the rheology of water ice [e.g., *Passey*, 1983]. Our results (Table 3) generally confirm and quantify the expectation that solids in the NH_3-H_2O system are very weak as they approach the 176 K peritectic and that partially molten material can have vanishingly low strength. On the other hand, we have concluded here that at temperatures below 140 K, dihydrate is as strong or stronger than water ice at laboratory strain rates. If this relationship stands up to the several orders of magnitude extrapolation to planetary strain rates, then water ice + dihydrate alloys on the surfaces of icy moons may have to be reinterpreted as explanations of tectonic features seen on these surfaces.

There are additional implications of the unusually high activation energy of dihydrate that need to be carefully considered, especially in near-surface environments where large temperature gradients exist. If the laboratory results are extrapolated to planetary strain rates, then the 6-order-of-magnitude range of viscosity of dihydrate accessible with only a 33-K range of temperature might be exploited to explain a variety of surface features. On Triton, for example, there is a great diversity of terrains and morphologies on one moon [*Smith et al.*, 1989]. Note also that this steep effect of temperature on dihydrate viscosity has potential for thermomechanical instability in icy satellites with endogenic heat sources. It also has the potential for faulting instabilities caused by shear heating. Finally, a number of models invoke a two-layer surface structure (hard above soft) on small satellites to explain coronae [*Janes and Melosh*, 1988], crater retention [*Passey*, 1983], and grooved terrain [*Herrick and Stevenson*, 1990]. The viscosity gradient across a single layer of dihydrate-rich material in an ordinary near-surface gradient may suffice for these models.

SUMMARY AND CONCLUSIONS

Laboratory experiments with ammonia + water mixtures of $x_{NH_3} \leq 0.295$ have confirmed earlier speculation about the weakness of these alloys at warm temperature and their ability to flow at very low viscosity in the partial melt regime, but our experiments have also revealed unexpected phase behavior and astonishing strength of the alloys at low temperatures. To summarize our findings:

1. The subsolidus flow of alloys of $0 \leq x_D \leq 1$ (x_D being the mole fraction dihydrate in a water ice + dihydrate alloy) is described by a single law of the form of equation (1) over the temperature range $143 < T < 176$ K. The flow law constants for representative values of x_D are given in Table 3. The two-phase flow model that matches our observations lies between a condition of uniform stress in both phases and a condition of uniform strain. Just below the 176-K peritectic, the pure water ice and dihydrate end-members of the two-phase mixture differ in strength by a factor of about 5 (about 4 orders of magnitude in viscosity), approximately independent of strain rate. At about 143 K the two phases have the same strength.

2. Ammonia dihydrate is the predominant NH_3-bearing phase in our samples, but both an amorphous phase and ammonia monohydrate have appeared at times, apparently metastably. The amorphous phase occurs regularly in as-molded ammonia-water solids but devitrifies readily upon pressurization to 50 MPa. Monohydrate invariably occurs, with an approximately equal amount of dihydrate, in samples of $x_{NH_3} = 0.05$. It occurs only in small amounts ($\leq$1–2%) in most $x_{NH_3} > 0.05$ samples, but in one anomalously (very) weak sample of $x_{NH_3} = 0.15$ (sample 223), it was more abundant than dihydrate.

3. Ammonia monohydrate may be weaker than dihydrate at the conditions of our experiments.

4. Partial melting in samples with an originally large volume fraction of dihydrate results in vanishingly low strengths, and the strength drop appears immediately at the peritectic temperature. However, at $x_{NH_3} \leq 0.05$ (melt volumes $\leq$15%), partially molten samples are not as dramatically weakened, and the strength loss is gradual as temperature is increased through and above the peritectic. There is not a simple relationship between volume of melt and strength loss.

5. At high differential stresses, water ice + dihydrate samples exhibit a shear instability that resembles transformational faulting in pure ice.

Acknowledgments. NASA support under order W-15,070 is gratefully acknowledged. This work was performed under the auspices of the U.S. Department of Energy by the Lawrence Livermore National Laboratory under contract W-7405-ENG-48.

REFERENCES

Bertie, J. E., and M. R. Shehata, Ammonia dihydrate: Preparation, x-ray powder diffraction pattern and infrared spectrum of $NH_3 \cdot 2H_2O$ at 100 K, *J. Chem. Phys.*, *81*, 27–30, 1984.

Boone, S., and M. F. Nicol, Ammonia-water mixtures at high pressures: Melting curves of ammonia dihydrate and ammonia monohydrate and a revised high-pressure phase diagram for the water rich region, *Proc. Lunar Planet. Sci. Conf.*, *21st*, 603–610, 1991.

Chan, J. P., and W. F. Giauque, The entropy of $NH_3 \cdot 2H_2O$: Heat capacity from 15 to 300 K, *J. Phys. Chem.*, *68*, 3053–3057, 1964.

Consolmagno, G. J., Ice-rich moons and the physical properties of ice, *J. Phys. Chem.*, *87*, 4204–4208, 1983.

Cooper, R. F., and D. L. Kohlstedt, Rheology and structure of olivine-basalt partial melts, *J. Geophys. Res.*, *91*, 9315–9323, 1986.

Croft, S. K., J. I. Lunine, and J. Kargel, Equation of state of ammonia-water liquid: Derivation and planetological applications, *Icarus*, *73*, 279–293, 1988.

Cynn, H. C., S. Boone, A. Koumvakalis, M. Nicol, and D. J. Stevenson, Phase diagram for ammonia-water mixtures at high pressures: Implications for icy satellites, *Proc. Lunar Planet. Sci. Conf. 19th*, 433–441, 1989.

Durham, W. B., H. C. Heard, and S. H. Kirby, Experimental deformation of polycrystalline H_2O ice at high pressure and low temperature: Preliminary results, *Proc. Lunar Planet. Sci. Conf. 14th*, Part 1, *J. Geophys. Res.*, *88*, suppl., B377–B392, 1983.

Durham, W. B., S. H. Kirby, and L. A. Stern, Effects of dispersed particulates on the rheology of water ice at planetary conditions, *J. Geophys. Res.*, *97*, 20,883–20,897, 1992.

Heard, H. C., W. B. Durham, C. O. Boro, and S. H. Kirby, A triaxial deformation apparatus for service at $77 \leq T \leq 273$ K, in *The Brittle-Ductile Transition in Rocks*, *Geophys. Monogr. Ser.*, vol. 56, edited by A. G. Duba, W. B. Durham, J. W. Handin, and H. F. Wang, pp. 225–228, AGU, Washington, D. C., 1990.

Herrick, D. L., and D. J. Stevenson, Extensional and compressional instabilities in icy satellite lithospheres, *Icarus*, *85*, 191–204, 1990.

Hildenbrand, D. L., and W. F. Giauque, Ammonium oxide and ammonium hydroxide: Heat capacities and thermodynamic properties from 15 to 300 K, *J. Am. Chem. Soc.*, *75*, 2811–2818, 1953.

Hogenboom, D. L., and J. S. Kargel, Ammonia-water densities and phase relations to four kilobars, *Lunar Planet. Sci.*, *XXI*, 522–523, 1990.

Janes, D. M., and H. J. Melosh, Sinker tectonics: An approach to the surface of Miranda, *J. Geophys. Res.*, *93*, 3127–3143, 1988.

Jankowski, D. G., and S. W. Squyres, Solid-state ice volcanism on the satellites of Uranus, *Science*, *241*, 1322–1325, 1988.

Kargel, J. S., S. K. Croft, J. I. Lunine, and J. S. Lewis, Rheological properties of ammonia-water liquids and crystal-liquid slurries: Planetological applications, *Icarus*, *89*, 93–112, 1991.

Kirby, S. H., Localized polymorphic phase transformations in high-pressure faults and applications to the physical mechanism of deep earthquakes, *J. Geophys. Res.*, *92*, 13,789–13,800, 1987.

Kirby, S. H., W. B. Durham, and H. C. Heard, Rheologies of ice I_h, II and III at high pressures: A progress report, in *Ices in the Solar System*, edited by J. Klinger et al., pp. 711–729, D. Reidel, Norwell, Mass., 1985.

Kirby, S. H., W. B. Durham, and L. A. Stern, Mantle phase changes and deep-earthquake faulting in subducting lithosphere, *Science*, *252*, 216–225, 1991.

Lewis, J. S., Satellites of the outer planets: Their physical and chemical nature, *Icarus*, *15*, 174–185, 1971.

Lewis, J. S., Low temperature condensation from the solar nebula, *Icarus*, *16*, 241–252, 1972.

Olovsson, I., and D. H. Templeton, The crystal structure of ammonia monohydrate, *Acta Crystallogr.*, *12*, 827–832, 1959.

Passey, Q. R., Viscosity of the lithosphere of Enceladus, *Icarus*, *53*, 105–120, 1983.

Prinn, R. G., and B. Fegley, Jr., Kinetic inhibition of CO and N_2 reduction in circumplanetary nebulae: Implications for satellite composition, *Astrophys. J.*, *249*, 308–317, 1981.

Rollet, A.-P., and G. Vuillard, Sur un nouvel hydrate de l'ammoniac, *C. R. Hebd. Seances Acad. Sci., Ser. A*, *243*, 383–386, 1956.

Schenk, P. M., Fluid volcanism on Miranda and Ariel: Flow morphology and composition, *J. Geophys. Res.*, *96*, 1887–1906, 1991.

Smith, B. A., and the Voyager Imaging Team, Voyager 2 at Neptune: Imaging science results, *Science*, *246*, 1422–1449, 1989.

Squyres, S. W., R. T. Reynolds, P. M. Cassen, and S. J. Peale, The evolution of Enceladus, *Icarus*, *53*, 319–331, 1983.

Stevenson, D. J., and J. I. Lunine, Mobilization of cryogenic ice in outer solar system satellites, *Nature*, *323*, 46–48, 1986.

Tullis, T. E., F. G. Horowitz, and J. Tullis, Flow laws of polyphase aggregates from end-member flow laws, *J. Geophys. Res.*, *96*, 8081–8096, 1991.

Van Kasteren, P. H. G., The crystallization behaviour and caloric properties of water/ammonia mixtures between 70 and 300 K, *Annexe Bull. Inst. Int. Froid*, *4*, 81–87, 1973.

W. B. Durham, Lawrence Livermore Laboratory, L-201, Box 808, Livermore, CA 94550.

S. H. Kirby and L. A. Stern, U.S. Geological Survey, 345 Middlefield Road, MS 977, Menlo Park, CA 94025.

(Received August 3, 1993;
revised May 20, 1993;
accepted June 9, 1993.)